Ultrasound in Med. & Biol., Vol. 30, No. 9, pp. 1119–1131, 2004

0301-5629/04/$–see front matter

ELSEVIER

doi:10.1016/j.ultrasmedbio.2004.07.011

● *Original Contribution*

A METHOD TO CREATE REFERENCE MAPS FOR EVALUATION OF ULTRASOUND IMAGES OF CAROTID ATHEROSCLEROTIC PLAQUE

J. E. WILHJELM,* M. S. JENSEN,* K. L. GAMMELMARK,* B. SAHL,† K. MARTINSEN,* J. U. HANSEN,* T. BRANDT,* S. K. JESPERSEN,‡ E. FALK,† K. E. FREDFELDT§ and H. SILLESEN‖

*Center for Arteriosclerosis Detection with Ultrasound (CADUS), Ørsted·DTU, Technical University of Denmark, Kgs. Lyngby, Denmark; †Institute of Experimental Clinical Research, Aarhus University Hospital (Skejby), Aarhus, Denmark; ‡Novo Nordisk A/S, Brennum Park, Hillerød, Denmark; §Department of Radiology, Frederiksund Hospital, Frederiksund, Denmark; and ‖Department of Vascular Surgery, Gentofte University Hospital, Hellerup, Denmark

Abtract—Ten formalin-fixed atherosclerotic carotid plaques removed by endarterectomy were molded into rectangular agar blocks containing fiducial markers on the top surface. Plaque and fiducial markers were imaged with 3-D multiangle ultrasound (US) spatial compounding as well as planar X ray. Subsequently, the blocks were decalcified, sliced, photographed and analyzed histologically. This gave a total of 123 slices. The plaque regions of the photographs were outlined and the outline adjusted to partly compensate for occasional displacement during slicing. Inside this outline, the material constitutions were found by incorporating the histologic information. From this set, slices with 1. too much tissue displacement due to cutting or 2. lack of identification of calcification as found by x ray, were removed. This resulted in 53 reference maps. The material types identified covered soft tissues, fibrous tissue, calcified tissue and unidentified tissues. The 53 reference maps can be used for direct automated quantitative comparison with US images. (E-mail: jw@oersted.dtu.dk) © 2004 World Federation for Ultrasound in Medicine & Biology.

Key Words: **Ultrasound, Spatial compounding, Atherosclerosis, Reference maps, X-ray, Density, Histology, Agar, Formalin fixation, Geometrical agreement.**

INTRODUCTION

Optimal treatment of atherosclerotic plaque in the carotid artery depends mainly on the classification of the lesions into two groups: Unstable plaque posing considerable future risk of creating embolism into the brain and stable plaques featuring little such risk (Grønholdt et al. 2001; Mathiesen et al. 2001; Polak et al. 1998). The unstable plaque is believed to have an atheromateous "gruel" (soft components) encapsulated from the blood stream by a relatively thin fibrous cap. This cap is likely to be rupture-prone. In more stable plaques, this cap is thicker and the relative volume of the atheromateous gruel is smaller (or absent) (Falk et al. 1995). Ultrasonic scanning is used routinely to diagnose and quantify lesions in the carotid arteries (Londrey et al. 1991; Sillesen et al. 1988), but detection of the above situation is still premature. Spatial compound imaging (Berson et al. 1981; Carpenter et al. 1980; Entrekin et al. 1999; Hernandez et al. 1996; Jespersen et al. 1998; Shattuck and Ramm 1982; Trahey et al. 1986) might be able to improve the accuracy of plaque evaluation, but this remains to be investigated.

To pave the way for quantitative investigations of the potentials of spatial compounding with respect to characterization of atherosclerotic lesions, this paper investigates the following questions:

1 Is it possible to create reference maps for formalin-fixed plaque specimens, against which previously recorded ultrasound (US) data can be compared quantitatively?
2 Will these maps show the main constituents of the plaque (e.g., lipid-rich tissue, fibrous rich tissue and calcified tissue)?
3 Can an estimate of the geometrical precision be given?

Ideally, a given reference map should show the different materials present in the associated scan plane of the US image, but with the (normally unproblematic) geometrical distortion present in the US image (due to

Homepage: http://www.oersted.dtu.dk/~jw/cadus
Address correspondence to: J. E. Wilhjelm, MS EE, PhD, Ørsted·DTU, Technical University of Denmark, Bldg. 348, Kgs. Lyngby DK-2800 Denmark. E-mail: jw@oersted.dtu.dk

spatially varying speed of sound). To elaborate on the latter, a geometrical "twist" of the plaque on the US image does not necessarily pose problems, as long as the plaque is categorized into the correct group, so that the choice of treatment is unaffected.

Previous studies have used histologic processing of atherosclerotic carotid plaque prescanned in vitro with US in an attempt to validate US-derived features of the plaque when comparing US images with the spatially associated histologic section (Arnold et al. 2000; Goes et al. 1990; Rakebrandt et al. 2000). However, neither decalcification nor problems with identifying calcified tissue from the histologic sections were mentioned (Arnold et al. 2000; Goes et al. 1990) or clearly identified as a major problem (Rakebrandt et al. 2000). With respect to spatial alignment, none of the studies applied spatial fiducial markers that marked each individual slice.

The present paper uses surgically removed formalin-fixed carotid plaque specimens for the purpose of creating reference maps at discrete locations over the entire plaque. To keep track of spatial alignment, the plaques were molded into an agar block containing fiducial markers before scanning with spatial compound US. Conventional x-ray images were also recorded for obtaining alternative assessment of calcification. This was followed by decalcification. By using the fiducial markers, each plaque was subsequently sliced, photographed and finally analyzed histologically at exactly the same planes as were imaged with US. The reference maps were then created with information from the anatomical photographs and the histologic information. Finally, reference maps not showing calcification as seen on the x-ray images were discarded.

MATERIALS AND METHODS

Ten atherosclerotic carotid plaques were obtained at carotid endarterectomy and selected randomly from a series of 119 consecutively operated patients who had experienced ipsilateral neurologic symptoms. All patients gave informed consent and the study protocol was approved by the medical ethics committee for Copenhagen and Frederiksberg counties (# KF 01-375/94).

The plaques were fixed in formalin and each plaque (or slice of a plaque) underwent exactly the same procedure, which is described below in chronological order.

Weight and volume measurements

The plaques were removed from formalin and rinsed in demineralized water. A suture was placed at the edge of the plaque and the plaque was subsequently put into a glass with demineralized water. Air in the water and on the plaque was removed (excavated) in vacuum.

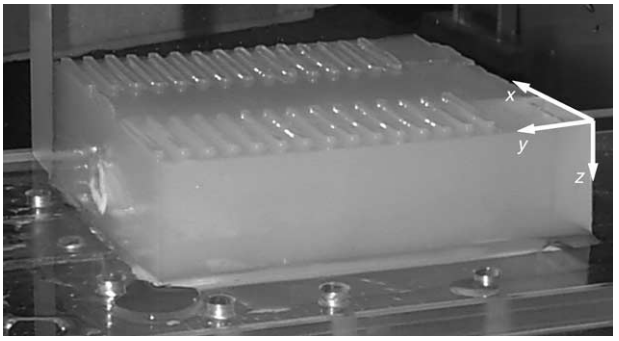

Fig. 1. Example of agar block with tissue (cut off at the left end to visualize the tissue sample) and fiducial markers on top of the block. Note the coordinate system to the right.

The weight of the glass with water, plaque and suture was found (Scaltec SBC31 scale, error below 0.001 g, much lower than the change in weight due to evaporation from the surface of the plaque). Next, the plaque was hung in the suture and the weight was found again. Finally, the plaque was removed from water and excess water was carefully removed with a soft napkin. Then, the weight of the plaque was found, $m(q)$. By means of Archimedes' principle, the volume of each plaque was also found, $V(q)$. The measurements were repeated the next day. The correlation between weight from one day to the next was $r \approx 0.99$. Likewise, the correlation was found for the two volume measurements.

Molding the plaque into an agar block

The plaque was subsequently placed (on a support made by two sutures) in an acrylic molding frame (inner dimension: 75 × 111 × 34 mm). Hot (45°C) degassed liquid agar (1% weight agar-agar in degassed demineralized water) was slowly poured into the frame. When filled, a lid with rows of rectangular openings was placed on top of the liquid agar. After the agar had solidified, the block contained two rows of fiducial markers on the top that both could be recognized by US and, later, by the operator who sliced the agar block. An example of a partly sliced agar block is shown in Fig. 1, which also shows the coordinate system used throughout this paper. The fiducial markers were 1.5 mm wide (in the y-direction) and spaced 2.5 mm in the y-direction.

When not in use, the agar block was kept in a container with demineralized water and rhodalon at 5°C.

Ultrasound scanning

The agar block with the plaque specimen was placed in a scanning tank with approximately 21°C demineralized, degassed water and cross-sectional images interspaced 0.5 mm (in the y-direction) were recorded by use of the Ørsted·DTU experimental com-

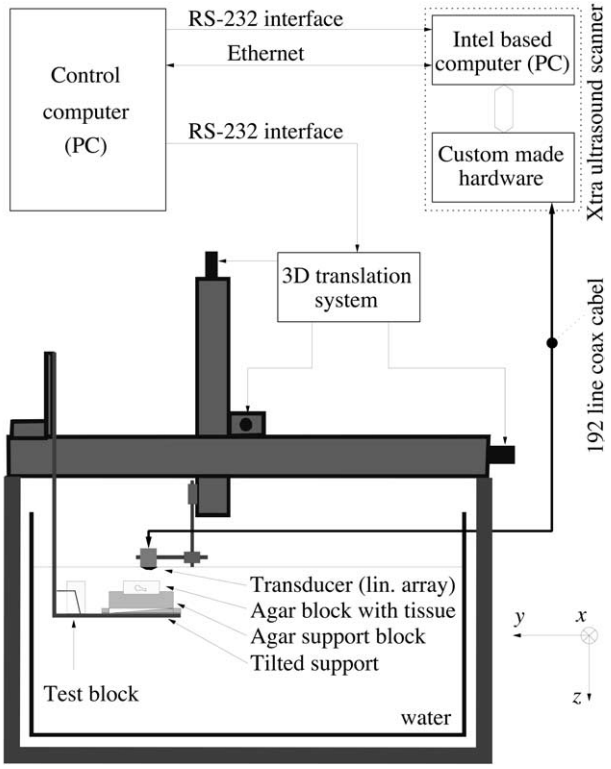

Fig. 2. Illustration of the ultrasound measurement system.

pound US scanner, the Xtra system (Jespersen et al. 1998), using a linear-array transducer with a center frequency of 7.5 MHz and the in-plane scanning angles: θ [element] [−21°, −14°, −7°, 0°, 7°, 14°, 21°]. The Xtra system operated by recording one single-element signal at a time. The distance from the transducer sole to the center of the plaque was 20 mm. At this depth, the axial and lateral −3-dB approximate widths of the point spread function were 0.15 and 0.5 mm, respectively. The −3-dB approximate width of the point spread function perpendicular to the images plane was 0.8 mm. The scan planes covered the entire plaque, and the number of planes ranged from 50 to 80. Scanning time was about 12 h and done overnight, when the level of external interference was the lowest. The setup is shown in Fig. 2. The envelope of the recorded (beam-formed) radiofrequency (RF) data were scan-converted to form raw single-angle images, $I_{us}(q, y, \theta; z, x)$, associated with angle θ and cross-sectional scan plane y. z and x constitute the image plane. Each image consists of 192 parallel scan lines. If the images are combined to a spatial compound image, then, as described previously (Jespersen et al. 1998), the fully compounded region (FCR) will be a triangle and, in this study, the majority of the tissue specimen was inside this triangular region. The US images presented in this paper (e.g., Fig. 5) are extracted as a rectangular region mainly located inside the FCR.

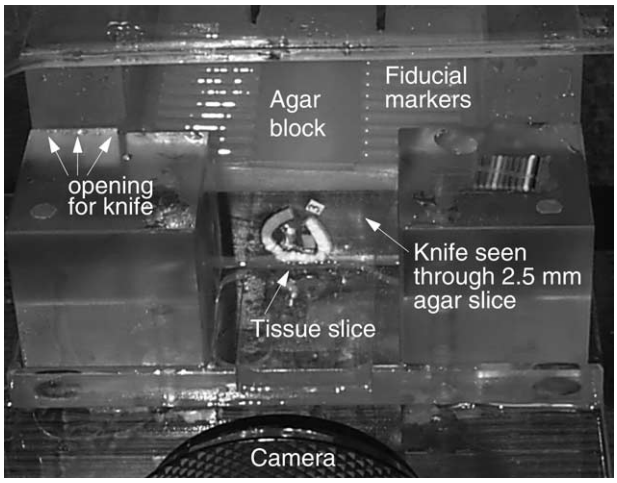

Fig. 3. Model photograph of an agar/tissue slice cut off from the end of the agar block, with the black knife still sitting behind the tissue slice. The lower part of the image shows the lens of the camera used to photograph the slice. The tissue shown here is porcine.

X-ray imaging

A projection x-ray image was taken of each agar block with plaque with a mammography unit (MAMEX dc®, Soredex, Helsinki, Finland). The tube voltage was 27 kV, distance tube to film was 600 mm, distance center of object to film was 30 mm. Distances on objects (at center of object) will then be about 5% smaller than they appear on the film. Filter was molybdinum 0.03 mm. Exposure time based on optical density was 3.8 s to 4.1 s. After this, a photograph was taken of the agar block with plaque, using a conventional optical camera. The photograph was taken from the top of the block and, therefore, appears the same way as the x-ray image.

Slicing of the agar block with plaque

To conduct both the slicing of the agar block with plaque and, later, the microtome slicing involved with the histologic analysis, the plaque had to be decalcified. The agar block with plaque was therefore placed in 0.33 mol/L EDTA under stirring for a period of 1 to 2 months.

Subsequently, the agar block was cooled to 5°C and then placed in a special slicing frame, in which the block could be sliced from the end with a slice thickness of 2.5 mm (in the y-direction), so that slicing planes were either through a fiducial marker or between two such markers. Care was taken not to compress or in other ways to deform the agar and plaque. The slicing was done with a trimming blade (Feather, Osaka, Japan) lubricated in glycerol to reduce the risk of tissue adhering to the blade.

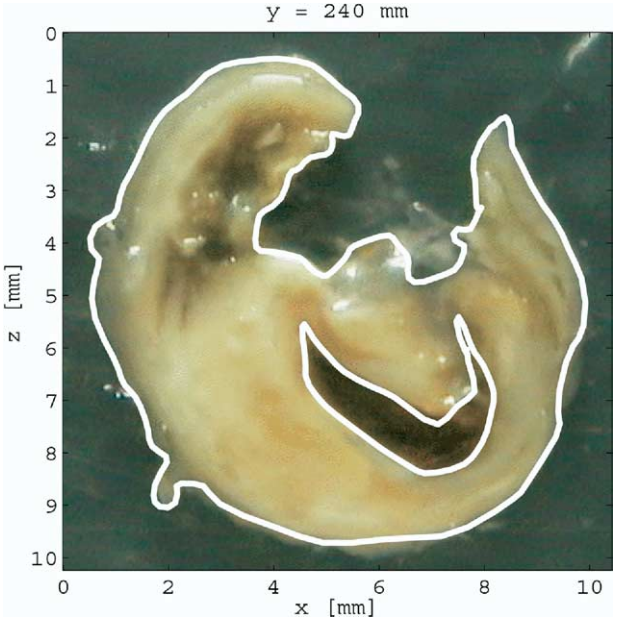

Fig. 4. The anatomical photograph for plaque 0, anatomical scan plane 5, $I_{ana}(q,y;\ x,z)$. The thick outline is denoted $O_{ana}(q,y;\ x,z)$.

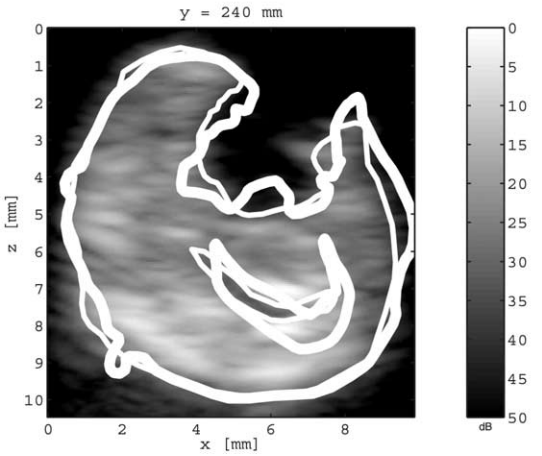

Fig. 5. The multiangle compound image, $I_{us,\,mean}(q,y;\ x,z)$, for the same scan plane as in Fig. 4. The thin and thick outlines correspond to those in Figs. 4 and 6. The thin outline is denoted $O_{us}(q,y;\ x,z)$.

Nevertheless, for some slices, the tissue deformed slightly during cutting. Immediately after the knife had cut through the tissue, the agar slice was marked with a small paper label with slice number and indication of whether the cutting plane was through a fiducial marker or between two. Next, the face of the 2.5-mm tissue slice was photographed, as illustrated in Fig. 3. An example of the resulting anatomical photograph is shown in Fig. 4. A calibration cross was later placed at the same distance from the camera to allow metric calibration of the anatomical photographs. The plaque/agar slice was then removed from the end of the agar block, trimmed and placed in a marked tissue cassette (with paper label still sitting on the agar), for later histologic analysis.

Histologic analysis

The 2.5-mm thick tissue slices were processed for high-quality microexamination (formalin-fixed paraffin sections). During this procedure, which included dehydration in alcohol, substitution with coconut oil and embedding in paraffin, all neutral lipids (free cholesterol, cholesterol esters and triglycerides) were extracted. Paraffin sections (5-μm thick) were cut on a microtome (from the surface that was photographed macroscopically), sampled on glass slides, deparaffinized, stained with elastin-trichrome, mounted and coverslipped. The glass slides were cut in size to fit into standard 35-mm slide frames and the images were then digitized. These digitized images were adjusted for malrotation and/or mirroring by comparing with their corresponding anatomical photographs.

Tissues shrink during dehydration and paraffin embedding and remain shrunken during the subsequent procedures. The degree of shrinkage depends on the type of tissue but amounts to approximately 30% area reduction (Baker 1958).

Tissue type identification via histologic analysis

The deparaffinized tissue sections were stained with elastin-trichrome staining, rendering elastic tissue black, collagen blue, and muscle cells and blood components (thrombus and hemorrhage) red. Lipids were extracted during the histologic processing and left behind unstained areas such as cavities (devoid of supporting collagen), foam cells, and so-called cholesterol clefts (extracted cholesterol crystals).

Because the plaques were decalcified before processing, it was not possible to identify and quantify calcification by staining specifically for calcium. Nevertheless, the prior presence of calcification (in vivo) may be inferred by the presence of a characteristic connective tissue matrix in the processed tissue (a compact matrix with special staining features).

As a consequence, the presence of calcification cannot always be identified. An area was only identified as calcified, if the pathologist was quite certain that it contained calcification. Thus, it is possible that some areas of calcification were overlooked.

The stained tissue sections were then analyzed visually by an experienced pathologist (unaware of the previous results) and the tissue types identified are shown in Fig. 8. “Material 1, thrombus (old and new)”

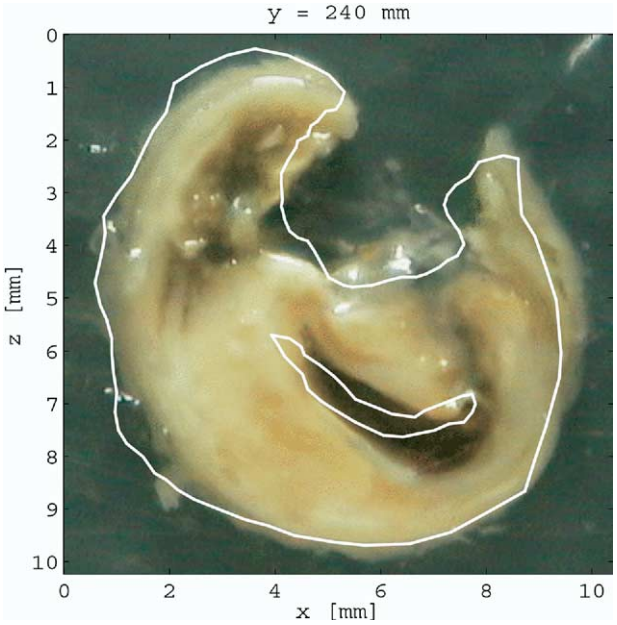

Fig. 6. The anatomical photograph from Fig. 4, with the US (thin) outline from Fig. 5 superimposed.

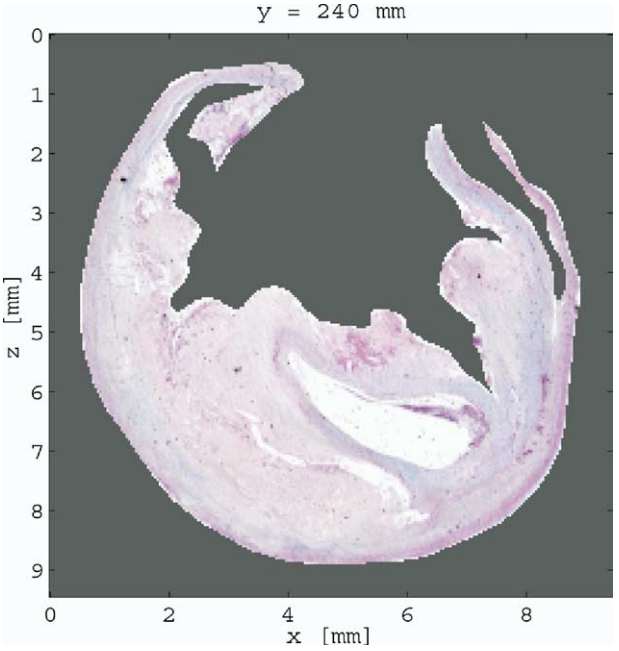

Fig. 7. The histologic image for the same scan plane as in Fig. 6, $I_{\text{hist}}(q,y;\ x,z)$.

represent blood factors, primarily platelets and fibrin with entrapment of cellular elements. The plaque specimens contained various amount of tunica media (material 6) which was removed together with the plaque during surgery. Material 8 is used to denote tissue that could not be classified, either because the region in the stained tissue image was indecisive or because the tissue was lost during the pathologic preparation. Loss of tissue could happen if the paraffinized tissue was cut slightly tilted or if it was too thin, so that it was lost in the water bath.

Creating the reference maps

The following method is explained by referring to Figs. 4 to 7, which show an US image, an anatomical photograph and a histologic image from exactly the same scan plane in the plaque.

Ideally, the reference map should be created directly from the histologic image. However, as exemplified in Fig. 7, this image is often strongly geometrically distorted (and shrunk) from the anatomical photograph in Fig. 6 (outlines are used later), which again can be geometrically distorted from the US image in Fig. 5. Similar observations have been made by Rakebrandt et al. (2000). To cope with these problems, the reference map was created with the following method.

The anatomical photographs were printed on paper and the outline of the tissue was manually drawn onto these, while looking at both the photograph and the open tissue cassette with the actual tissue slice. The outline was drawn to ensure that only tissue in the cutting plane was included in the outline(s). The outline was subsequently drawn on the digitized anatomical photograph. An example is seen in Fig. 4 (thick outline).

The anatomical outline was then copied to the associated spatial compound US image and offset so as to match the image as well as possible, subjectively judged by visual inspection, as illustrated in Fig. 5 (thick outline). Normally, this outline did not completely match the US image, mainly due to tissue displacement during cutting/slicing and geometrical distortion occurring with diagnostic US (e.g., due to variations in speed of sound). The lack of geometrical match can be seen in the example in Fig. 5, when the thick outline is compared to the contours of the US image.

Then, when needed, segments of the (thick) outline were moved so that the entire outline matched the contours of the US image as well as possible. The position and shape of a segment of a thick outline was only adjusted radically when it was obvious that the deviation was due to tissue displacements during slicing. Care was taken to keep constant the area of the entire outline. The resulting outline (thin outline) can be seen in Fig. 5.

This modified (thin) outline was finally reimposed on the anatomical photograph, as show in Fig. 6. The reference map was then created by outlining the individual tissue types directly on the computer screen showing the content of Fig. 6. Tissue types and location were identified based on both the anatomical photograph (Fig. 6) and the histologic image (Fig. 7). The regions were

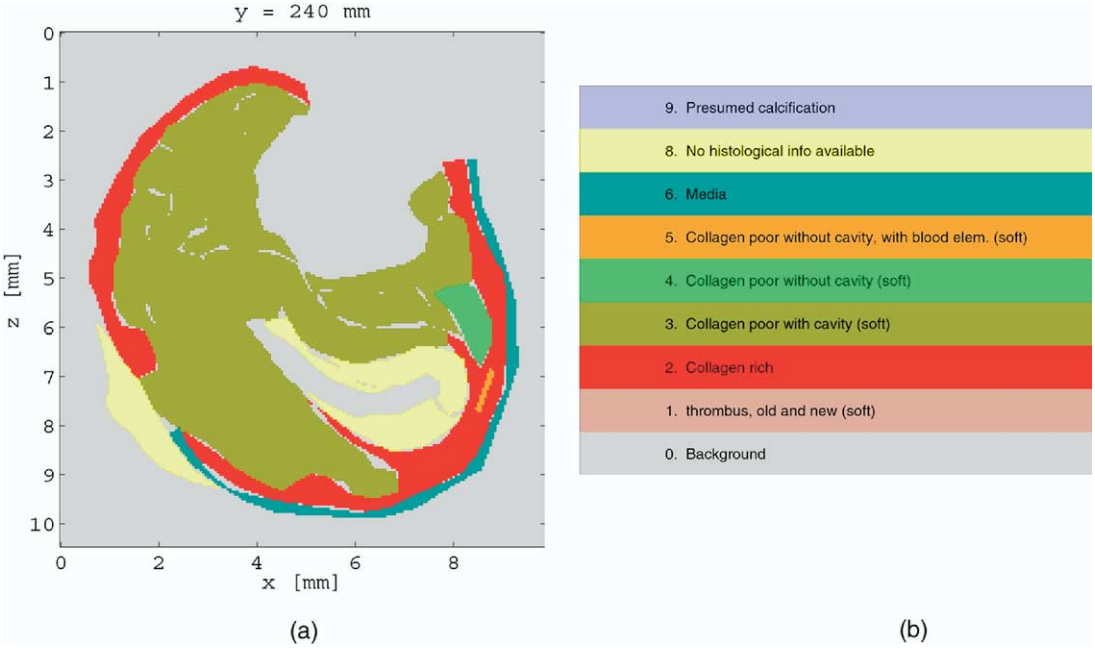

Fig. 8. (a) The reference map, $I_{ref}(q,y;\ x,z)$, corresponding to the US image in Fig. 5. (b) Corresponding colors showing the different tissue types identified histologically in this study. Material 7 is reserved for other use and does not exist here. "Soft" identifies the four tissue types that are considered "soft tissues."

placed, taking account of the displacement of the thin outline in Fig. 6, relative to the contour of the tissue. The histologic images were viewed as slides on a large projector screen and in a microscope. The final reference map corresponding to this example is seen in Fig. 8.

Note that material 3 (collagen-poor with cavity) in Fig. 8 covers what appear to be different materials in Fig. 6. In the latter figure, some of the tissue contains bleeding. However, material 3, "collagen poor with cavity," was not subdivided into tissues with and without blood components. The reason is that both collagen-poor and blood components were believed to be echolucent tissues.

RESULTS

A total of 10 plaques were processed, yielding from 10 to 16 slices per plaque. This gave a total of 123 slices each with associated US data, anatomical photograph, histologic image and, thereby, reference map.

In an attempt to verify the reference maps in terms of geometry and content (whether or not the material identified on the reference map is the correct material), they were compared geometrically with the anatomical outline and content-wise with the x-ray images. These and some other supporting comparisons were done as illustrated in Fig. 9.

Identification of fiducial markers

Figure 10 shows a photograph of one of the plaques in the agar block, seen from the top. To visualize the appearance of the fiducial markers in the US data, Fig. 11 shows a C-scan created from the entire 3-D US data set.

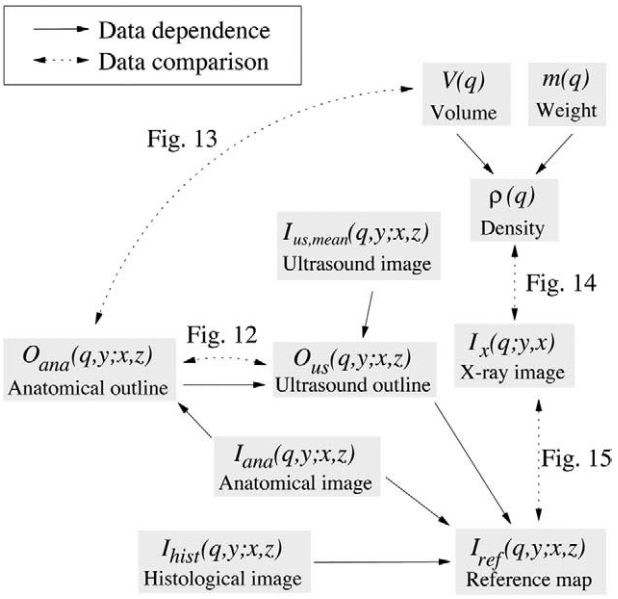

Fig. 9. Overview of the data involved in obtaining the reference maps and the subsequent verification. Definitions are listed in the Nomenclature section.

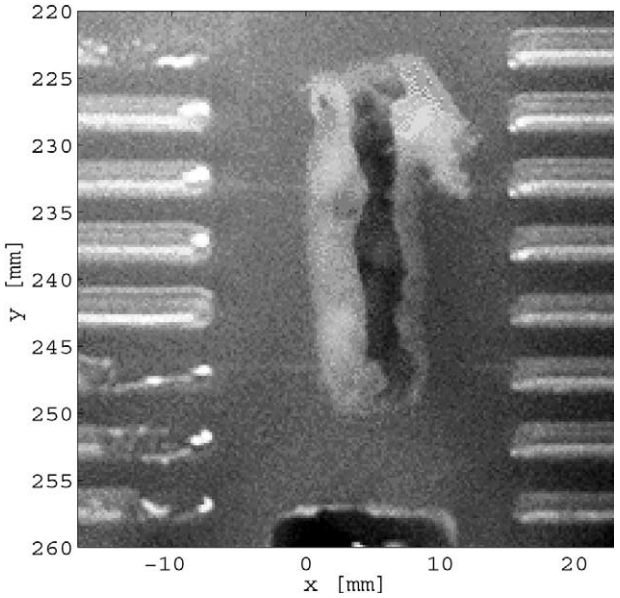

Fig. 10. Photograph of the plaque in the agar block.

The plane of the C-scan is parallel with the surface of the agar block (*x-y* plane) and is located halfway between the agar surface and the surface of the fiducial markers. The light gray area in the middle of the bottom of the image is the edge of the filling hole (for liquid agar), which makes it possible to exactly identify each (otherwise identical) fiducial marker. The precise locations of the fiducial markers were identified by finding the best match of a grid consisting of eight parallel lines (along the x-axis) spaced 5 mm.

Geometrical investigations

Figure 12 shows how well the anatomical photographs agree with the US images, for all plaques pooled together (i.e., 123 slices). Specifically, the figure shows the relative number of overlapping pixels for the outer outline of the reference map, $O_{us}(q,y;\ x,z)$, and the outlines drawn on the anatomical photographs, $O_{ana}(q,y;\ x,z)$. This is the same as the relative overlap between the thin and thick outline in Fig. 5 (87% in this particular case). Inspection of Fig. 12 yields that 41 of the 123 slices agree by more than 90%. The average agreement was 85%. The areas of the two outlines were nearly identical (on average, the area of $O_{us}(q,y;\ x,z)$ was 2.5% smaller than the area of $O_{ana}(q,y;\ x,z)$).

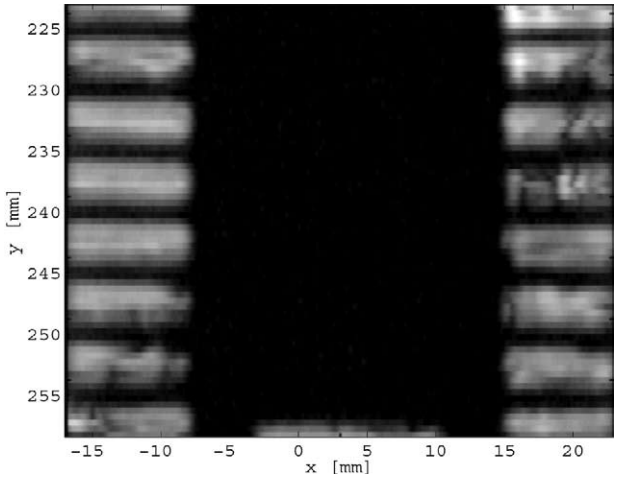

Fig. 11. The fiducial markers identified by US on the surface of one of the agar blocks.

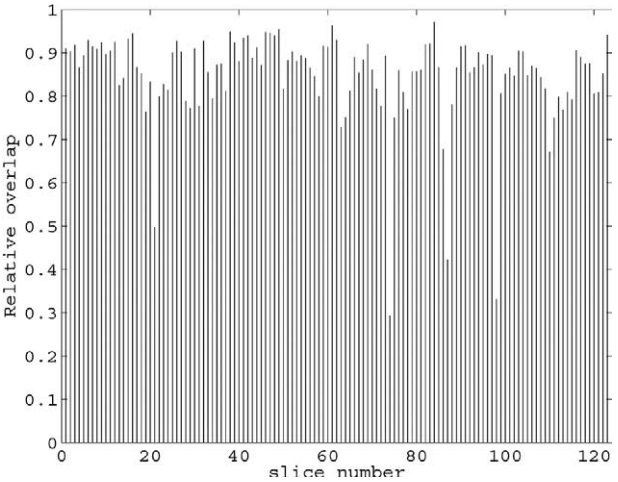

Fig. 12. Geometrical agreement (relative overlap) between reference maps and anatomical photographs.

To get a further indirect measure of the correctness of the area of the outlines of the anatomical photographs, Fig. 13 compares the volume of the plaques obtained directly, *V(q),* with the volume calculated based on the outlines of the tissue on the anatomical photograph. The latter is calculated from an estimate of the volume between the slice faces. Because the slope of the regression line is close to unity, the volume of a plaque measured from the anatomical photographs is, on average, 0.23 cm^3 larger than the volume measured directly.

Content investigations

The plaques were decalcified before the histologic analysis. However, traces of calcification can, to some (unknown) extent, be identified on the latter. Thus, the only relatively firm knowledge of calcification is based on the x-ray images. Before using the x-ray images, the physically measured density was compared to the relative calcification estimated from the x-ray images. As partly demonstrated by Walker et al. (2002), because calcified tissue has a higher physical density than lipid and fibrous tissue, the two measures should be positively correlated.

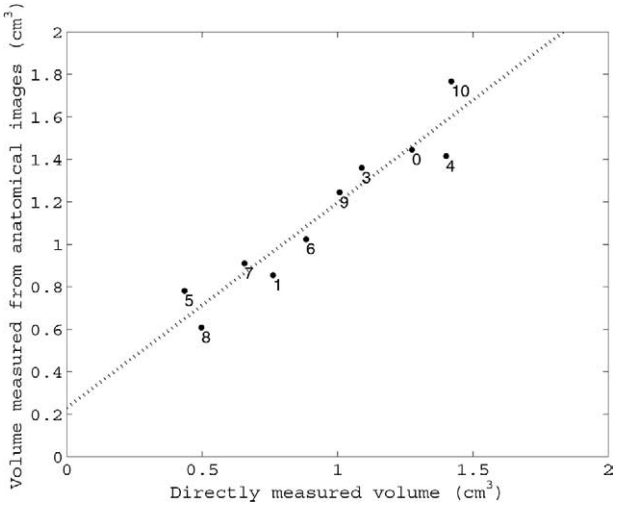

Fig. 13. Volume measured physically vs. volume measured from outline of tissue on the anatomical photographs.

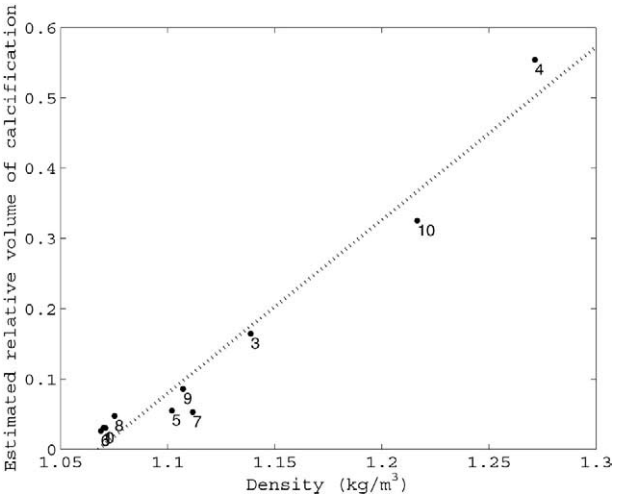

Fig. 14. Directly measured density vs. relative volume of calcification, as estimated from the x-ray images.

The estimated relative volume of calcification was found this way. The thickness of plaque q, (measured along the z-axis) was found from the reference map, and "a thickness image" in the x–y plane was calculated. Specifically, if $L_{\text{ref}}(q,y;\ z,x)$ is unity, when $I_{\text{ref}}(q,y;\ z,x) > 0$ and 0 otherwise, the thickness image, $D(q,y,x)$ can be written as

$$D(q,y,x) = \sum_z L_{ref}(q,y;z,x)\Delta z. \tag{1}$$

For completeness, $\sum_x \sum_y D(\text{q,y,x})\Delta x \Delta y$ is approximately the volume of plaque q. Δx, Δy and Δz are the physical distances between the centers of two neighboring voxels in the indicated directions. This thickness image overlay the x-ray image (both images have the same metric axes and were offset to match quite exactly). Then, if a pixel in the x-ray image was considered to be "white" (i.e., above a preset threshold), then the associated tissue in the entire column of voxels inside the plaque (along the z-axis) was considered to be calcified. The relative content could then be calculated. Because it is unlikely that all voxels in a column in the z-direction are calcified, this approach will yield an overestimation of relative content of calcification. Finally, note that the threshold was verified visually, but the value was not critical to the results.

The result is presented in Fig. 14, which reveals a good correlation. Notice the relatively high level of "estimated relative volume of calcification."

As stated previously, one cannot be sure to identify all calcified regions from the histologic images. On the other hand, if a region is identified as calcified on the histologic images, then there is a very high likelihood that this region is indeed calcified. Thus, such a region should be matched by a white area at the corresponding location in the associated x-ray image. To investigate this, all 10 x-ray images were compared to the associated 10 reference data sets. Specifically, an x-ray image was compared to a projection of the corresponding reference map created by:

$$I_{ref.proj}(q;y,x) = \begin{cases} 0, & \text{if } I_{ref}(q,y;z,x) = 0, \quad \text{for all } z \\ 1, & \text{if } 0 < I_{ref}(q,y;z,x) < 9, \quad \text{for all } z \\ 3, & \text{if } I_{ref}(q,y;z,x) = 9, \quad \text{for all } z \end{cases}. \tag{2}$$

The three values correspond to background, soft tissue and calcified tissue, respectively. An example of an image set, where most calcification appears to be detected by histology, is given in Fig. 15a and b. Another plaque, where quite a bit of calcification seems to have disappeared in the histologic process, is given in Fig. 15c and d. Note the low spatial sampling rate in (a) and (c).

Identifying usable reference maps

Based on the previous results, it is now possible to identify those reference maps that can be used as reference for the US images: Of the total of 123 slices, 78 slices contained no calcification on either histology data or x-ray images. Eight slices contained calcification on both histology data and x-ray images. Finally, the remaining 37 slices contained calcification identified by x-ray images only. This is shown in Fig. 16a. Removing the slices with less than 85% area agreement (Fig. 12) yields the result in Fig. 16b. Finally, removing the slices containing more than (e.g.,) 15% of the unidentified material 8 gives the result in Fig. 16c. This eventually

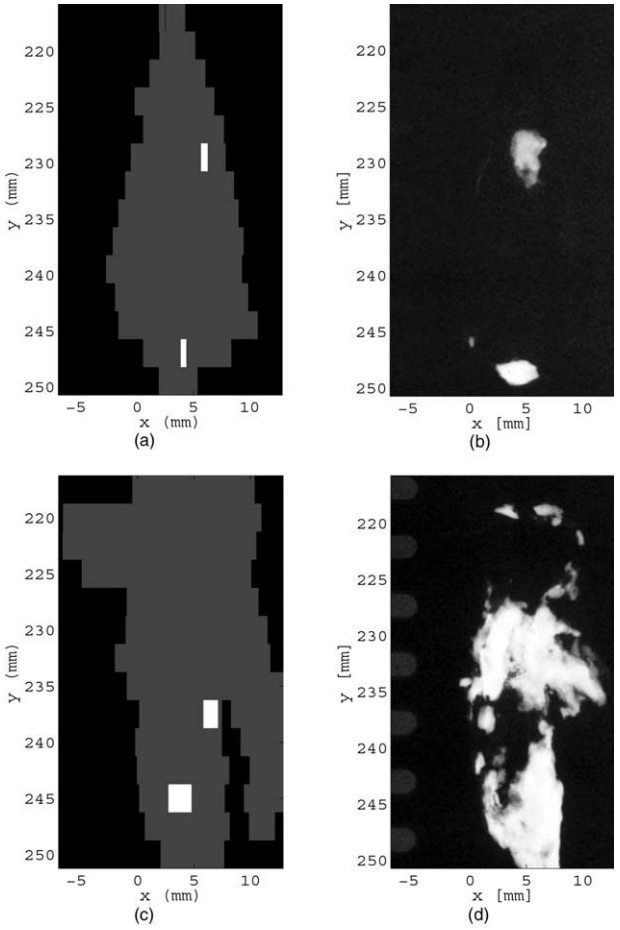

Fig. 15. (a), (c) Calcification (white) identified by histology plotted on plaque contour (dark gray) according to eqn (2); (b), (d) Corresponding planar projection x-ray images recorded of plaque in agar block (before calcification). White areas in x-ray images are assumed to represent calcification. (a), (b) A situation where most calcification seems identified by histology; (c), (d) the case for another plaque, where quite a bit of calcification seems to have disappeared in the histologic process.

indicates that a total of 23 + 1 = 24 slices are of sufficiently high quality that they can be used as a (pixel-to-pixel) reference for the corresponding US images.

An alternative measure of the outcome is given in Table 1 which shows the total area of reference information. Specifically, for each material, this table shows the number of regions as well as their total area for all the slices in Fig. 16b that are indicated as black and white. The same information is also provided for the case where an "ultrasound uncertainty band" of width 2.5λ around the periphery of each region is removed. λ = 0.2 mm at 7.5-MHz transducer frequency and 2.5λ is roughly the width of the −3-dB point spread function in the *x*-direction.

It can be observed, from Table 1, that tissue types

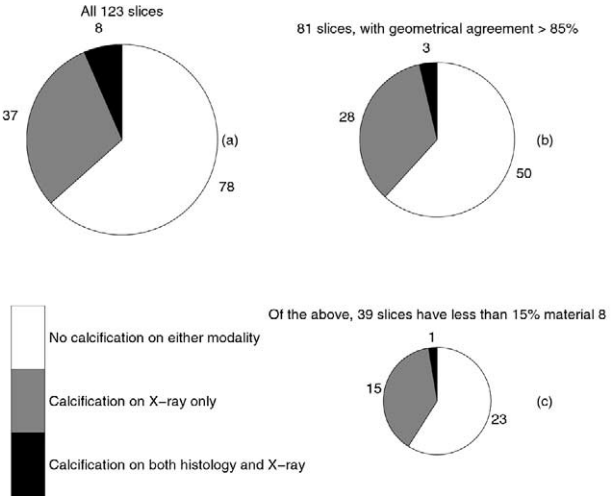

Fig. 16. Overview of useable reference maps, when imposing various quality requirements.

that typically appear dark on US images (tissue types 1, 3, 4 and 5) represent 30% of the area, and tissue types that typically appear bright (tissue types 2, 6 and 9) represent 50% of the area.

DISCUSSION

The individual comparisons

Fiducial markers and slicing. With the distance of 0.5 mm between US scan planes used in this study, Fig. 11 shows that the fiducial markers are clearly visible in the US data. Thus, the identification of the locations of the US scan planes at fiducial markers and between fiducial markers is associated with a maximum error of 0.25 mm. The precision of the slicing afterward is more difficult to assess, but it is estimated that any part of the anatomical photograph plane is maximally 1 mm from the correct plane.

Overlap between ultrasound and anatomical outline. Figure 12 shows an average agreement of 85% with just four scan planes exhibiting agreement below 50% (where the plaque "capsized" during slicing). In general, the better the agreement, the more precise is the cutting of the plaque. However, there might be a small contribution to geometrical distortion due to spatial variations in the speed of sound in the plaque/water medium. However, with a geometrical agreement above 85%, it can probably be assumed that displacement during cutting was low and that geometrical distortion of the US image was also low.

Physical volume vs. volume measured from anatomical photographs. Figure 13 shows a quite good correlation between the directly measured volume and the vol-

Table 1. Area and number of regions for the 10 plaques, based on only those slices where geometrical agreement is larger than 85% and where calcification has been identified both histologically and with x ray

	Full region		Excluding a 2.5λ uncertainty band	
Material	Area λ^2	Regions	Area λ^2	Regions
9 Presumed calcification	205	5	93	1
8 No histological information available	10,843	146	5147	29
6 Media	5571	79	5162	2
5 Collagen-poor with blood elements (soft)	1180	57	838	3
4 Collagen-poor without cavity (soft)	9138	99	4001	24
3 Collagen-poor with cavity (soft)	7467	50	3324	18
2 Collagen-rich	19,798	139	8233	43
1 Thrombus, old and new (soft)	207	2	61	1
Total	54,409	577	26,859	121

ume estimated from the anatomical outlines. There is an off-set, however, which can be because:

- The area of the anatomical outlines depends on the possible misalignment mentioned above. The correct area is equal to the minimum area, obtained when all slice faces of a plaque are strictly parallel. Any misalignment will give rise to an area that is too large.
- Some tissue types shrink when fixed in formalin (Schned et al. 1996; Weind et al. 2000; Wisecarver 1999), even although such observations are not fully consistent (Dalager-Pedersen et al. 1999). Differences can be due to tissue type and methodology. If the present plaques underwent shrinkage due to the formalin fixation, there is a possibility that this shrinkage was partially reversed by the permanent decrease in formalin concentration that began when the plaques were encapsulated in agar.
- When the plaques were molded into 45°C hot agar, there is a possibility of swelling, which did not reverse when the temperature subsequently decreased to 21°C.
- The liquid agar can enter into small cracks in the surface of the plaque that are not found and outlined in the anatomical photograph. This could possibly also have happened in the hemorrhage region on Fig. 4.

Density vs. relative volume of calcification estimated from x-ray images. The result in Fig. 14 shows a quite good correlation between measured density and relative content of calcification in the plaques. In the method used, it is likely that too many voxels are considered to be calcified, but this will be the case for most of the plaque, thus resulting in a consistent overestimation. Specifically, the relative volume of calcification is probably not as high as up to 60%, as suggested in Fig. 14.

X-ray images vs. collapsed reference maps. The example in Fig. 15 shows that quite a bit of calcification might be missed by the histologic analysis. Thus, x-ray images had to be used in classifying the slices into useable and nonusable in Fig. 16. Due to its high density, calcification has a large influence on the US image (e.g., high echogenicity and shadows on deeper-lying plaque structures) and thus needs to be identified.

Identifying usable reference maps. From Fig. 16, 24 maps can be identified as usable with the given precision requirements. If the presence of material 8 was acceptable, there would be 53 maps. For these 53 maps, Table 1 shows how much "reference area" the method of this work provided. With a 30%:50% ratio between echopoor and echogenic tissue types, the different materials are well represented with respect to comparisons with US data.

Limitations and methodological considerations

The method developed in this work is a tool that can be used in the design of new US methods aimed at identifying or classifying different tissues. As a tool, it is relevant to compare the cost of making it with the outcome.

The cost of the tool is mainly the labor involved with: molding the tissue into agar, slicing the tissue, making the histologic analysis, digitizing and analyzing the images and, finally, drawing and modifying all the outlines on the anatomical photographs, on the US images and on the reference maps.

The outcome can be measured in how much square lambda reference information is available for the different tissue types identified, as indicated in Table 1. The outcome should also be considered in terms of the precision of the reference maps. This is difficult to assess with the present method, but a conservative estimate is that the location of the outline is correct within $\approx \pm$ 2.5λ, subjectively judged from the outline drawing.

It is noted that the tissue used in this work was formalin-fixed. Ultrasound classification methods devel-

oped with this kind of tissue will not necessarily give the same results as would be obtained in vivo. Of particular interest is that, because of temperature-dependent phase changes of lipid (Lundberg 1985), lipid and fibrous tissue might not feature the same differences in backscattering level in vivo at 37°C compared with the situation in formalin-fixed condition at 20°C.

The outline of an anatomical photograph was plotted on the corresponding US image and then modified to match the contour of the latter. This way, the US outline will tend to cover the same area on the US image, as if the outline was drawn only on the US image, without the knowledge of the anatomical photograph. The latter is the case in clinical investigations involving outlining of plaque on US images (El-Barghouty et al. 1996; Wilhjelm et al. 1998). With this approach, geometrical distortions due to the US measurement situation are somewhat accounted for.

Improvements of the method

To make the reference maps more correct in terms of geometrical precision, material identification and to obtain more reference area, a number of improvements could be envisioned.

One of the major problems is the inability to safely identify calcified tissue from the histologic image, as also noted by Rakebrandt et al. (2000). Because x-ray-based computerized tomography (CT) images reveal absolute absorption of x-rays within the spectral band used, which (for soft tissue) is proportional to electron density in the tissue investigated, this technique should have good potential in measuring the location and degree of calcification in plaque (Estes et al. 1998). Therefore, a possible improvement would be to make a 3-D CT scan of the plaques while they are in agar (and before decalcification). These density data could then be combined with the histologic data. It would be necessary to scan the entire agar blocks so that the fiducial markers would appear and it would probably be beneficial to embed some fiducial markers in the agar block for precise alignment, test of geometry and evaluation of resolution size (Kaufman et al. 2003). In addition, ideally, each agar block should contain small chambers with known concentrations of calcium to verify the recorded Hounsfield units and to estimate the relative content of calcium in the calcified regions. Eventually, CT could be used after decalcification to verify proper removal of calcium.

The slicing of the agar block with plaque should also be improved, so that the geometrical alignment is maintained above 90%. It can probably not be better, due to the geometrical distortions present with diagnostic US. A more precise cutting might be easier to accomplish, if the atheromateous part of the plaque were more strongly fixed to the surrounding biologic tissue than is the case here. If, for instance, completely occluded atherosclerotic femoral arteries were used, then the plaque could be removed with the surrounding artery. With the arterial wall covering the plaque, less geometrical deformity might result when cutting the plaque.

When the tissue is cut, both faces of a cut should be photographed. The latter should be done with a flat-bed scanner to facilitate a very high sampling rate and to avoid geometrical distortions in the anatomical photograph.

Another limitation is that the histologic image (thickness of 5 to 10 μm) is assumed to represent an US scan plane that originates from a tissue region with a -3-dB width in the order of 0.8 mm, as also pointed out by Rakebrandt et al. (2000). This could, in principle, be overcome by paraffin-embedding the entire plaque and cutting it every, e.g., 0.1 mm (instead of every 2.5 mm). However, this would give a 25-fold increase in data, which would require automated analysis methods.

Another aspect that ought to be investigated is the orientation parameters of anisotropic tissue (e.g., collagen-rich tissue) because, for this kind of tissue, the level of backscattering of US might depend on the angle of insonification. In the present case of large complex atheromateous plaques, however, the orientation parameters might be quite complex, compared with the situation of measuring backscattering from media and adventitia of mildly arteriosclerotic aorta walls, as has previously been studied by Picano et al. (1985).

Finally, the different tissue constituents are not completely separated from each other in the way suggested by the reference maps of this study (e.g., Fig. 8). More often, overlap regions of lipid and fibrous tissue exist, as also noted by Arnold et al. (2000).

CONCLUSIONS

The results of the present study show that it is possible to create reference maps for formalin-fixed plaque specimens, with which previously recorded US data can be compared quantitatively. The maps show the main constituents of the plaque, such as soft tissues, fibrous tissue and calcified tissue. The method involves removal of a substantial amount of reference maps that do not fulfill a set of quality requirements using the current technique. The uncertainty of the location of these maps is estimated to be within $\approx \pm 2.5\lambda$ at a transducer frequency of 7.5 MHz.

These reference maps allow automated quantitative comparison of different techniques for processing the recorded US data, thus providing a tool for measuring the performance of different tissue-characterization techniques.

Acknowledgements—CADUS is supported by the Danish Technical and Medical Research Councils. The authors gratefully acknowledge

the help of N. Nyssen in obtaining the density of the plaque, for which S. Nielsen, Pilot Plant, Technical University of Denmark, is also acknowledged. The authors also gratefully acknowledge the help by Dr. M. M-L. Grønholdt, KAS Gentofte, Hellerup, for providing access to the plaque specimens. The authors also thank Associate Professor Mikael Jensen, Department of Mathematics and Physics, The Royal Veterinary and Agricultural University, Frederiksberg, for fruitful discussions. Finally, the inputs of the anonymous referees are appreciated.

NOMENCLATURE

s	Scan plane number
$V(q)$, $m(q)$	The volume and the weight of plaque q, respectively
$I_{us}(q,y\theta\ z,x)$	The US image for plaque q, scan plane y, beam angle θ and image coordinates z, x
$I_{us,\,mean}(q,y;\ z,x)$	The multiangle compound image for plaque q, scan plane y and image coordinates z, x; this is obtained by averaging $I_{us}(q,y\theta\ z,x)$ over all θ
$O_{us}(q,y;\ z,x)$	The outline corresponding to the US image for plaque q, scan plane y and image coordinates z, x
$I_{ana}(q,y;\ z,x)$	The anatomical photograph for plaque q, scan plane y and image coordinates z, x
$O_{ana}(q,y;\ z,x)$	The outline corresponding to the anatomical photograph for plaque q, scan plane y and image coordinates z,x
$I_{hist}(q,y;\ z,x)$	The histologic image for plaque q, scan plane y and image coordinates z,x
$I_x(q;y,x)$	The x-ray (projection) image for plaque q and image coordinates y,x
$I_{ref}(q,y;\ z,x)$	The reference map for plaque q, scan plane y and image coordinates z,x; the outer outline of $I_{ref}(q,y;\ z,\ x)$ is identical to $O_{us}(q,y;\ z,\ x)$
$L_{ref}(q,y;\ z,x)$	Unity, when $I_{ref}(q,y;\ z,x) > 0$ and 0 otherwise
$D(q,y,x)$	Thickness of plaque q in the z-direction
Slice	Plaque slice of 2.5-mm thickness in the y-direction
Section	Plaque slice of 5 to 10-μm thickness in the y-direction

REFERENCES

Arnold A, Taylor P, Poston R, Modaresi K, Padayachee S. An objective method for grading ultrasound images of carotid artery plaques. Ultrasound Med Biol 2000;27(8)1041–1047.

Baker JR. Principles of biological microtechnique. London, UK: Methuen, 1958:75–86.

Berson M, Roncin A, Pourcelot L. Compound scanning with an electrically steered beam. Ultrason Imaging 1981;3:303–308.

Carpenter DA, Dadd MJ, Kossoff G. A multimode real time scanner. Ultrasound Med Biol 1980;6:279–284.

Dalager-Pedersen S, Falk E, Ringgaard S, Kristensen I, Pedersen E. Effects of temperature and histopathologic preparation on the size and norphology of atherosclerotic carotid arteries as imaged by MRI. J Magn Reson Imaging 1999;10:876–885.

El-Barghouty NM, Levine T, Ladva S, Flanagan A, Nicolaides A. Histological verification of computerised carotid plaque characterisation. Eur J Vasc Endovasc Surg 1996;11:414–416.

Entrekin R, Jackson P, Jago JR, Porter BA. Real time spatial compound imaging in breast ultrasound: Technology and early clinical experience. Medicamundi 1999;43:3:35–43

Estes JM, Quist WC, Lo Gerfo FW, Costello P. Noninvasive characterization of plaque morphology using helical computed tomography. J Cardiovasc Surg 1998;39:5527–534

Falk E, Shah PK, Fuster V. Coronary plaque disruption. Circulation 1995;92(3):657–671.

Goes E, Janssens W, Maillet B, et al. Tissue characterization of atheromatous plaques: Correlation between ultrasound image and histological findings. J Clin Ultrasound 1990;18:611–617.

Grønholdt ML, Nordestgaard BG, Schroeder TV, Vorstrup S, Sillesen H. Ultrasonic echolucent carotid plaques predict future strokes. Circulation 2001;104(1):68–73.

Hernandez A, Basset O, Chirossel P, Gimenez G. Spatial compounding in ultrasonic imaging using an articulated scan arm. Ultrasound Med Biol 1996;22(2):229–238.

Jespersen SK, Wilhjelm JE, Sillesen H. Multi-angle compound imaging. Ultrason Imaging 1998;20:81–102.

Kaufman L, Mineyev M, Carlson J, Goldhaber D, Rumberger J. Coronary calcium scoring: modelling, predicting and correcting for the effect of CT scanner spatial resolution on Agatston and volume scores. Phys Med Biol 2003;48:1423–1436.

Londrey GL, Spadone DP, Hodgson KJ, et al. Does color-flow imaging improve the accuracy of duplex carotid evaluation? J Vasc Surg 1991;13(5):659–663.

Lundberg B. Chemical composition and physical state of lipid deposits in atherosclerosis. Atherosclerosis 1985;56:93–110.

Mathiesen EB, Bonaa KH, Joakimsen O. Echolucent plaques are associated with high risk of ischemic cerebrovascular events in carotid stenosis: The Tromso study 3. Circulation 2001;103(17): 2171–2175.

Picano E, Landini L, Distante A, et al. Angle dependence of ultrasonic backscatter in arterial tissues: A study in vitro. Circulation 1985; 72:3:572–576

Polak JF, Shemanski L, O'Leary DH, et al. Hypoechoic plaque at US of the carotid artery: An independent risk factor for incident stroke in adults aged 65 years or older. Cardiovascular Health Study. Radiology 1998;208(3):649–654.

Rakebrandt F, Crawford DC, Havard D, Coleman D, Woodcock JP. Relationship between ultrasound texture classification images and histology of atherosclerotic plaque. Ultrasound Med Biol 2000; 26(9):1393–1402.

Schned AR, Wheeler KJ, Hodorowski CA, et al. Tissue-shrinkage correction factor in the calculation of prostate cancer volume. Am J Surg Pathol 1996;20(12):1501–1506.

Shattuck DP, Ramm OTv OTv. Compound scanning with a phased array. Ultrason Imaging 1982;4:93–107.

Sillesen H, Bitsch KR, Schroeder T, et al. Pulsed multigated Doppler ultrasonography in the diagnosis of carotid artery disease. Stroke 1988;19(7):846–851.

Trahey GE, Smith SW, Ramm OTv OTv. Speckle pattern correlation with lateral Aperture translation: Experimental results and implications for spatial compounding. IEEE Trans UFFC 1986;33(3):257–264.

Walker LJ, Ismail A, McMeekin W, et al. Computed tomography angiography for the evaluation of carotid atherosclerotic plaque: Correlation with histopathology of endarterectomy specimens. Stroke 2002;33:977–981.

Weind KL, Ellis CG, Boughner DR. Porcine aortic valve cusp dimensional changes with aldehyde fixation (Abst.). Canad J Cardiol 2000;16:110F.

Wilhjelm JE, Grønholdt M-LM, Wiebe B, et al. Quantitative analysis of ultrasound B-mode images of carotid atherosclerotic plaque: Correlation with visual classification and histological examination. IEEE Trans Med Imaging 1998;17(6):910–922.

Wisecarver JL. Allowing for shrinkage (Abstr.). Am J Gastroenterol 1999;94(7):1743.